Genome instability footprint under rapamycin and hydroxyurea treatments

Jing Li[1,2], Simon Stenberg[3], Jia-Xing Yue[1,2], Ekaterina Mikhalev[4], Dawn Thompson[4], Jonas Warringer[3] and Gianni Liti[2,5,*]

Affiliations:

[1]State Key Laboratory of Oncology in South China, Collaborative Innovation Center for Cancer Medicine, Sun Yat-sen University Cancer Center, Guangzhou, China; [2]Université Côte d'Azur, CNRS, INSERM, IRCAN, Nice, France; [3]Department of Chemistry and Molecular Biology, University of Gothenburg, Gothenburg, Sweden; [4]Ginkgo Bioworks, Boston, MA 02210 USA; [5]Lead Contact.

*Correspondence: gianni.liti@cnrs.fr

Key words:

Mutation rates, drift, selection, aneuploidy, LOH, drug resistance

Summary

The mutational processes are jointly shaped by genetic backgrounds, environments and their interactions. Accurate quantification of mutation rates and spectra under drugs has important implications in disease treatment. Here, we used yeast mutation accumulation lines (MALs) to profile the genome-wide mutational footprints of two chemotherapy drugs across multiple genetic backgrounds. Together with time-resolved phenotyping, we investigated the mutagenic effects of rapamycin and hydroxyurea and the associated functional implications. In the absence of drug treatment, we observed genetic backgrounds variation in point mutation rates. In rapamycin, we observed comparable or lower mutation rates than in the untreated control. However, we identified frequent chromosome XII amplifications, which compensated for rapamycin induced rDNA repeat contraction on this chromosome and thereby served to maintain rDNA content homeostasis. In hydroxyurea, we detected pervasive mutation rate elevation independent of genetic backgrounds, with high occurrence of aneuploidy that associated with dramatic fitness loss. Hydroxyurea induced a high T-to-G transversion rate that reversed the common G/C-to-A/T bias in yeast, a broad range of structural variants and a mutation footprint consistent with mechanisms of error-prone polymerase activities and NHEJ repair pathways. Taken together, our study provides an in-depth view of mutation rates and signatures in rapamycin and hydroxyurea and their impact on cell fitness, which brings insights for assessing their long-term effects on genome integrity.

Introduction

Genome instability, referring to the acceleration of mutation accumulation, is typified by specific mutational signatures[1]. Such signatures can be shaped by external factors, such as drug treatments, that target different aspects of the cellular machinery. Understanding why particular mutations occur and how they vary between individuals or environments is fundamental to widen our knowledge of the underlying mechanisms of mutagenesis[2,3]. However, accurate estimation of mutation rates and profiling of mutational signatures in specific environments are challenging to achieve. This is partially because of the confounding effects of selection, which favors some variants over others and thereby affects their frequency and likelihood of detection. Additionally, a continuous spatio-temporal record of cell populations during experimental evolution is hard to obtain, which makes it difficult to track the alteration of genetic and phenotypic properties during evolution. Therefore, it is crucial to examine mutational signatures and their phenotypic consequences under conditions where selection can be minimized, and in a time-resolved manner.

The budding yeast *Saccharomyces cerevisiae* is a classic, single-celled, eukaryotic model organism that can be easily manipulated and controlled in the lab. Asexually reproducing populations of yeast can be propagated in the lab for thousands of generations as Mutation Accumulation Lines (MALs). This experimental evolution protocol minimizes selection by repeatedly forcing cell populations through bottlenecks of random, single cells and mutations are therefore accumulated in a largely unbiased way. Intermediate stages of MALs evolution can be stored in freezers, ensuring that a fossil record of the evolving cells is preserved. The coupling of MALs with the usage of highly parallelized cell growth phenotyping platforms and whole-genome-sequencing allows to

monitor the fitness trajectories of the lines and to reconduct them to genomic alterations accumulating over time[4–8]. Yeast MALs have been used to estimate mutation rates and spectra for common lab strains in rich medium[9,10], as well as the effects of controlled variation in ploidy[11–14] and of some specific disruptions in the DNA repair/replication machinery[15,16]. However, mutational patterns can be also shaped by environmental factors, such as drugs and diet[17–21], and may differ between genetic backgrounds[22]. So far, systematic studies that explore the mutational landscape under stress conditions, particularly long-term anticancer treatments, are lacking.

Here, we compared the mutation profiles of 96 mutation accumulation lines (MALs), derived from 10 distinct genetic backgrounds, that were evolved for a total of ~181,440 generations in a drug-free (rich medium; YPD) condition, stressful hydroxyurea (HU) and rapamycin (RM) conditions. HU and RM represent two distinct mechanisms of action of chemotherapeutic treatments: impairing DNA repair/replication and inhibiting the TOR signaling in proliferating cells, respectively. The mutation rates and spectra of these two drugs were highly distinct at both nucleotide and structural levels, and this had direct effects on cell fitness. Our study represents an effective approach for the assessment of mutagenic risks of drugs and the understanding of their long-term effects.

Results

Mutation accumulation under HU but not RM impairs cell growth

To avoid confounding effects from working with a single and potentially atypical genetic background, we selected ten diploid *S. cerevisiae* genetic backgrounds and propagated MALs in hydroxyurea (HU) 10 mg/ml, rapamycin (RM) 0.025 µg/ml and drug-free rich medium (YPD, as control) (Fig. 1a, Table S1). The 10 genetic backgrounds comprised four homozygous representatives of diverged *S. cerevisiae* lineages[23] (WA: West African, WE: Wine/European, NA: North American, SA: Sake), as well as six heterozygous hybrids obtained through pairwise crosses of their haploid offspring (WA/WE, NA/WE, NA/WA, SA/WE, SA/WA, SA/NA) (Fig. 1b). The growth of these 10 genetic backgrounds varied under drug exposures (Fig. 1b, Tables S2-S4). The mean cell doubling time increased by 43.2% (standard deviation (sd) across strains=5.6%) and 38.1% (sd=16.0%) in HU and RM respectively compared with drug-free medium. Correspondingly, the mean absolute cell yield declined by 70.3% (sd=11.01%) in HU and 77.3% (sd=4.7%) in RM. Most strains show viability of 77.2% (sd=21.5%) and 94.7% (sd=7.9%) in HU and RM relative to in YPD.

We evolved four replicates for each of the 10 genetic backgrounds over 120 single-cell bottlenecks in YPD and 60 single-cell bottlenecks in HU and RM, corresponding to approximately 2760, 1200 and 1320 consecutive cell divisions respectively for each condition. Hereafter, we use the nomenclature “strain-condition–replicate” to represent each MAL. Cells of two homozygous genetic backgrounds (WA/WA, WE/WE) showed extremely low viability in HU and RM and another two (SA/SA and SA/WA) recurrently went extinct across all replicates in HU for repeated passages through single-cell bottlenecks (Fig. 1b). Excluding the lines above, therefore, there are a total of 40, 24 and 32 surviving MALs in YPD, HU and RM (Table S1). We stored all the MALs at five

intermediate stages of evolution to generate frozen fossil records (single-cell bottleneck 0, 30, 60, 90, 120 in YPD; single-cell bottleneck 0, 15, 30, 45, 60 in HU and RM). For each of the 96 surviving MALs, we established a dense cell growth record by measuring the cell doubling time and yield as proxies for fitness over the course of evolution (Fig. 1c, Supplementary Fig. 1 and 2, Table S2). In YPD, the cell doubling time remained stable for all the MALs (mean 1.44 h *vs.* 1.43 h at the initial and last time points respectively, Mann–Whitney U test, $p = 0.49$, sd = 0.046 h *vs.* 0.097 h), while the cell yield declined moderately (mean $\log_2$ normalized cell yield = 0.35 *vs.* 0.07 at the initial and last time points, $p = 0.01$, sd = 0.25 *vs.* 0.50). The yield decline was largely due to four lines (Supplementary Fig. 2a) becoming *petite* (i.e., forming very small colonies, which is a signature of respiration deficiency) and one line becoming haploid (Fig. 2a). The properties of cell growth in HU and RM evolved in different directions (Fig. 1d). Cell growth was seriously impaired during HU evolution, with doubling time becoming longer (mean doubling time 2.06 h *vs.* 2.42 h, Mann–Whitney U test, $p = 6.80\times10^{-7}$, sd = 0.11 *vs.* 0.37) and the normalized cell yield decreasing (0.82 *vs.* -0.24, $p = 1.15\times10^{-3}$, sd = 0.67 *vs.* 1.59), indicating the accumulation of strongly deleterious mutations. This fitness loss was strongest in the earliest stages of evolution (mean doubling time = 2.06 h *vs.* 2.23 at the initial and single-cell bottleneck 15, Mann–Whitney U test, $p = 0.009$) and then slowed substantially (mean doubling time = 2.23 h vs. 2.42 h at bottlenecks 15 and 60, Mann–Whitney U test, $p = 0.059$). In contrast, no fitness loss was observed during RM evolution, with doubling time unchanged (mean = 1.99 h vs. 2.03 h, Mann–Whitney U test, $p = 0.16$, sd = 0.26 *vs.* 0.22) and the cell yield improving (mean = 0.15 *vs.* 0.46, $p = 1.18\times10^{-4}$, sd = 0.38 *vs.* 0.56). We note that these trajectories across random single cell passages stand in stark contrast with the same lineages evolving adaptively in large cell populations under HU and RM exposure[8] (mean cell doubling time of adapted clones appearing after ~50 generations = 1.91 h and 1.48 h in HU and RM respectively). Both HU and RM evolved MALs consistently became less fit in the drug-free condition (Fig. 1c, $p < 8.11\times10^{-5}$, Supplementary Fig. 3), reflecting the accumulation of deleterious mutations. We therefore conclude that our MALs experienced no or only weak selection. We noted that the cell viability increased in YPD and HU (Fig. 1b, 1.37-fold and 1.75-fold increase), which was due to unavoidable selection against mutations decreasing viability during the single-cell bottlenecks. Taken together, the single cell passages resulted in a largely neutral evolution and the accumulation of deleterious mutations that impaired cellular fitness.

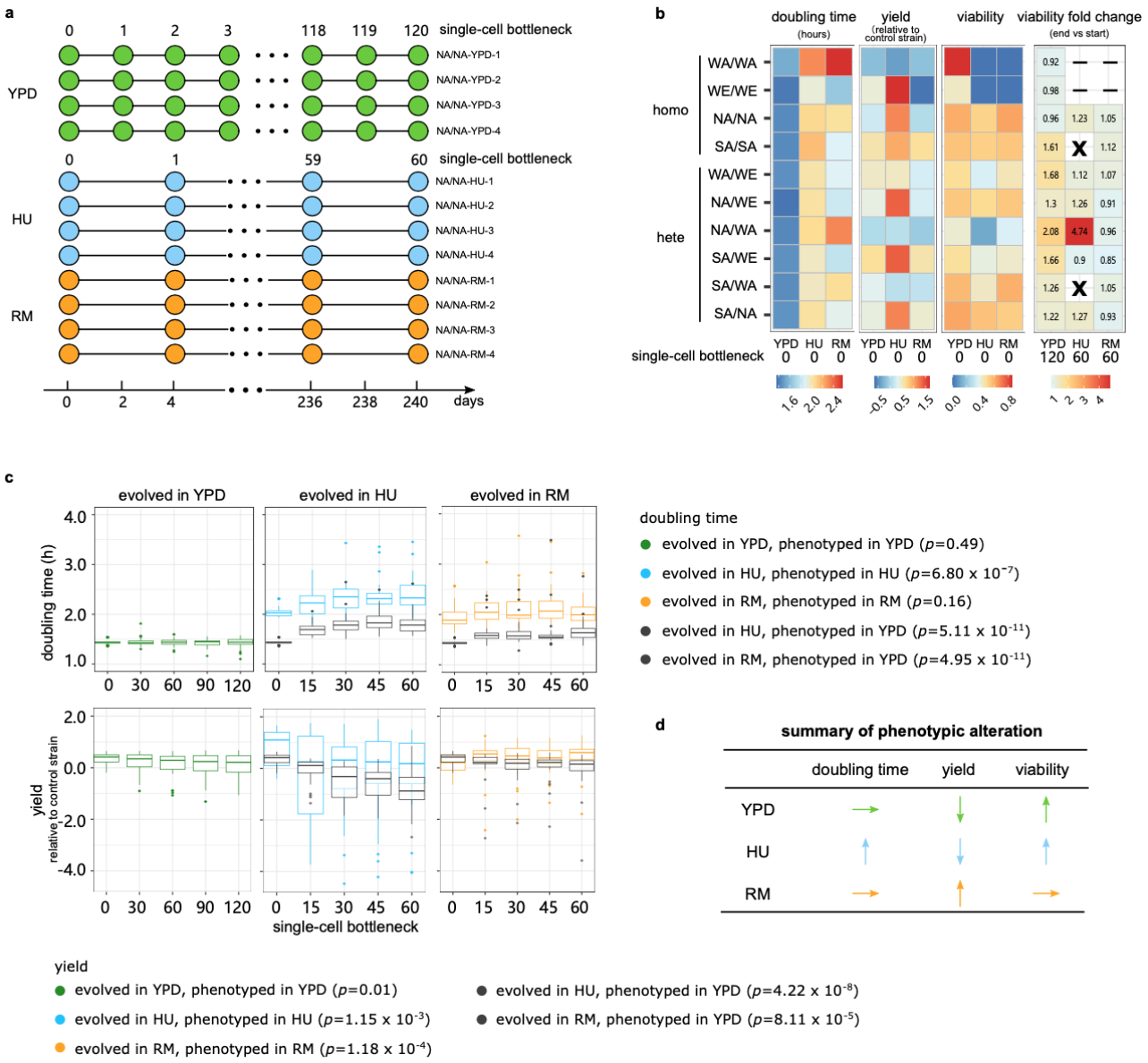

Figure 1. Mutation accumulation lines (MALs) design and fitness. (a) We evolved MALs in YPD (control), HU (hydroxyurea) and RM (rapamycin) for a total of 120 (YPD) and 60 (HU and RM) single-cell bottlenecks. The ten genetic backgrounds included four diploid homozygous strains (WA/WA - West African, WE/WE - Wine/European, NA/NA - North American, and SA/SA - Sake) and six hybrids derived from them. For each strain, we initiated 4 replicated MALs in each condition. These are named as "strain-condition–replicate", with e.g., "NA/NA-YPD-1" denoting the North American homozygote, evolved in YPD, replicate 1. Green, blue and orange circles represent the MALs in YPD, HU and RM respectively. The NA/NA genetic background MALs overview is shown as example. **(b)** Heatmap show the cell doubling time (hours), cell yield (log_2 cell yield normalized to that of the spatial control strain, NA/WA) and cell viability. Cell viability in YPD is represented as CFU^{YPD} counted cells, while cell viability in HU and RM is calculated as $CFU^{HU\ or\ RM}/CFU^{YPD}$). "X" indicates MALs with all four replicates going extinct. "-" indicates strains exclusion because of extremely low fitness in that condition. **(c)** Evolution of cell doubling time and yield. Boxplots show the cell doubling time and yield in drug and drug-free conditions (see legend) across the single-cell bottleneck (x-axis). Center line: median; box: interquartile range (IQR); whiskers: 1.5×IQR; dots: outliers beyond 1.5×IQR. The *p* value is measured by Mann–Whitney U test by comparing phenotypes at the initial and last timepoints of evolution. For each condition, the number of MALs included in the analysis (*N*) is N_{YPD}=40, N_{HU}=24, N_{RM}=32. **(d)** Qualitative summary of the direction in which each fitness proxy changes during the MALs.

Recurrent chromosome XII amplification under RM treatment maintains rDNA homeostasis

RM inhibits cell growth by restricting the activity of cellular master regulator TOR (Target of Rapamycin), but whether this restriction has mutagenic effects *per se* is unclear. We sequenced the MALs evolving in RM and compared the mutation spectrum to that of the YPD condition. We first focused on whole chromosome and large segmental copy number variants and structural variants. Ten out of 40 MALs (25%) evolved in YPD had at least one whole-chromosome gain or loss (Fig. 2a), corresponding to 1.38×10^{-4} events/MAL/generation, which is similar to previous reports on the S288C lab strain evolved in YPD[10,11] (Mann–Whitney U test, $p>0.16$). No significant difference in the aneuploidy rate was observed among the genetic backgrounds. These results suggest that the basal aneuploidy rate is essentially conserved across *S. cerevisiae* lineages. Among the ten MALs with aneuploidies, five acquired one extra chromosome, three acquired two or more different chromosomes, one acquired two extra chromosome I (chrI tetrasomy) and one lost a chromosome I (chrI monosomy). The WE/WE-YPD-4 accumulated four whole chromosomal copy number changes, which were unlikely to occur independently ($p=5.94\times10^{-4}$, Poisson distribution test) and represented connected mutational events[24]. The NA/WE-YPD-4 halved its ploidy and became a euploid haploid with recombined chromosomes (shown together with the LOH profile in Supplementary Fig. 8), reflecting that it passed through meiosis (sporulation and germination). This is surprising given the rich access to nutrients that normally precludes passage through meiosis. Globally, chromosome gains (13 events) outnumbered losses (2 events), agreeing with previous findings[10,11,14,25]. The two chromosome loss events were restricted to the smallest chrI. Assuming similar rates of chromosome gains and losses, this bias against chromosome deletion reflects selection against deleterious chromosome hemizygosity during evolution.

In RM, the rate of aneuploidies (4.21×10^{-4} events/line/generation) was >2-fold higher than in YPD, when excluding the unfit NA/WA-RM-4 line that underwent whole genome duplication and subsequent multiple chromosome losses (Fig. 2a, Supplementary Figs. 1, 2 and 4). A highly disproportionate fraction (64.7% in RM vs 6.7% in YPD, Fisher's exact test, $p=9.54\times10^{-4}$) of these aneuploidies corresponded to chromosome XII (chrXII) gains. Excluding these chrXII duplications, RM treatment did not alter aneuploidy rates (1.55×10^{-4} in RM *vs.* 1.38×10^{-4} in YPD, $p=0.89$). We also observed amplifications of chrXII right arm in NA/WE-RM-4, spanning the rDNA-array locus and associating to an inversion of the centromeric region (Fig. 2b). RM has been reported to repress rDNA repeat amplification and lead to contraction of the rDNA repeat cluster[26]. We therefore hypothesized that complete or partial chrXII aneuploidies could both be compensations that evolved to counteract deleterious repeat contractions of the rDNA locus. To test this, we estimated the rDNA copy number for all the MALs from sequencing read coverage. Under drug-free condition, the rDNA copy number in MALs with normal chrXII remained unchanged (Fig. 2c upper panel, mean rDNA copy number per chrXII normalized by the ancestors: 1.04). In contrast, the rDNA copy number per chrXII decreased in both HU and RM conditions (Mann–Whitney U test, $p<0.001$), consistent with loss of rDNA repeats in stress. Moreover, MALs with chrXII duplications had fewer rDNA repeats per chrXII than those with normal chrXII copy numbers (0.70 vs. 0.87 in HU, 0.66 vs. 0.76 in RM). Taken together, the above results support that duplication

of the entire chrXII and of the rDNA repeat containing segments of chrXII are compensatory responses to RM induced rDNA repeat contraction (Fig. 2c lower panel).

One interpretation of the above compensation mechanism is that rDNA repeat contraction is detrimental and the compensatory chrXII duplication is beneficial to cells in RM. However, we found the cell doubling time in RM to be unaffected by chrXII copy number (Fig. 2d, RM evolved MALs with chrXII gain, 1.99 h vs. 2.05 h at initial and last time points, p=0.43 and those without chrXII gain, 1.95 h vs. 2.03 h, p=0.09) while cell yield was weakly affected (RM evolved MALs with chrXII gain, 0.24 *vs.* 0.55 at initial and last time points, p=0.01 and those without chrXII gain, 0.28 *vs.* 0.48, p=0.09). All the RM-evolved MALs bear a fitness cost in drug-free condition independent of chrXII copy number. We therefore conclude that chrXII gain is not adaptive in RM *per se* but is an evolutionary conserved response to constrained expansion of rDNA repeats because of long-term RM treatment. This is also underscored by that the adaptive RM evolution of large cell populations of the very same lineages was driven by *TOR1* and *TOR2*[8] mutations rather than chrXII duplication. We also confirmed that the chrXII duplication in RM did not destabilize the genome, because the rates of other types of mutations, i.e., SNVs, INDELs and LOH, all remained unaffected (mutation rates of MALs with chrXII gain *vs.* without chrII gain, Mann–Whitney U test, p>0.23). Thus, chrXII duplication is unlikely to have caused the rDNA repeat contractions.

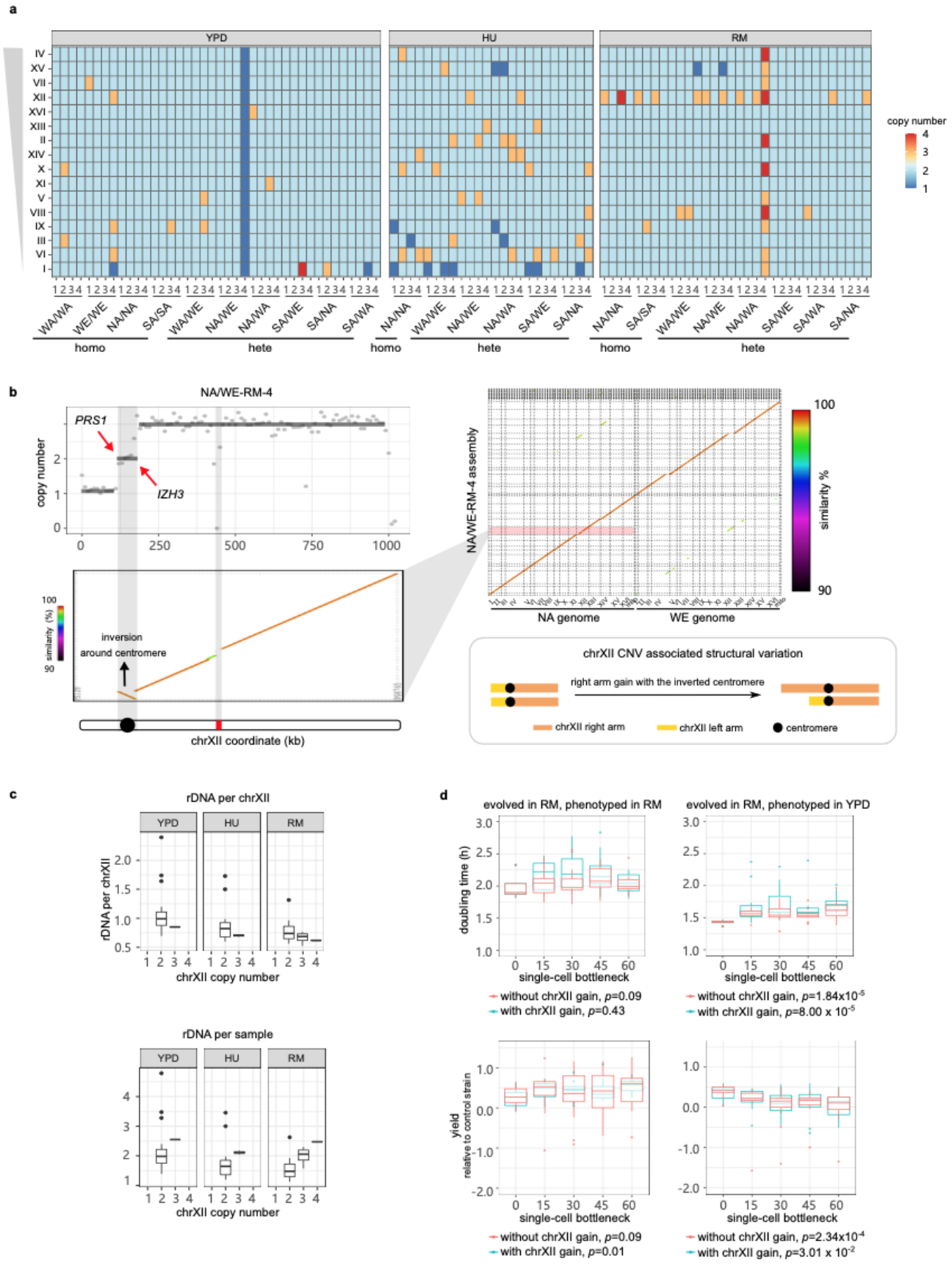
a
YPD
HU
RM
copy number
homo
hete
b
NA/WE-RM-4
PRS1
IZH3
copy number
inversion
around centromere
similarity (%)
chrXII coordinate (kb)
NA/WE-RM-4 assembly
NA genome
WE genome
similarity %
chrXII CNV associated structural variation
right arm gain with the inverted centromere
chrXII right arm
chrXII left arm
centromere
c
rDNA per chrXII
rDNA per chrXII
chrXII copy number
rDNA per sample
chrXII copy number
d
evolved in RM, phenotyped in RM
evolved in RM, phenotyped in YPD
doubling time (h)
single-cell bottleneck
without chrXII gain, p=0.09
with chrXII gain, p=0.43
without chrXII gain, p=1.84x10-5
with chrXII gain, p=8.00 x 10-5
yield
relative to control strain
without chrXII gain, p=0.09
with chrXII gain, p=0.01
without chrXII gain, p=2.34x10-4
with chrXII gain, p=3.01 x 10-2

Figure 2. ChrXII amplification compensates for rDNA contraction in RM. (a) Aneuploidies identified in the MALs. Dark blue indicates chromosome loss and orange/red indicates chromosome gain. The chromosomes are sorted by their size with larger chromosomes on the top. **(b)** Upper left, the short read sequencing revealed segmental CNV on chrXII of NA/WE-RM-4. The red arrows indicate the breakpoint of each segmental CNV. Upper right, the dot plot was generated by aligning the assembly from long-read sequencing to the reference genome. The x-axis represents NA and WE reference genomes. The y-axis represents the assembled contigs of NA/WE-RM-4 obtained from long read sequencing. Lower left, the zoom-in dot plot shows the contig of chrXII with an inversion. The bar below represents chrXII, with black circle and red rectangle indicating centromere and rDNA repeats respectively. Lower right, we propose the possible outcome of this CNV-associated inversion: the extra copy of chrXII right arm together with the centromere was inverted and replaced the original left arm. **(c)** rDNA copy number per chrXII (upper panel) and rDNA copy number per sample (lower panel) normalized by the ancestors for different strains, which were binned based on the evolved condition and the copy number of chrXII. Boxplot: center lines = median; boxes = interquartile range (IQR); whiskers =1.5×IQR; points = outliers beyond 1.5×IQR. **(d)** Cell doubling time (upper panel) and yield (lower panel) of RM-evolved MALs phenotyped with (left) or without (right) RM. The blue and red boxplots represent MALs with and without chrXII gain respectively. The *p* value was calculated to compare the cell doubling time and yield between the initial and last timepoint populations by Mann–Whitney U test.

HU broadly elevates CNV rates

HU induced DNA replication stress is widely accepted to lead to rampant genome instability[27,28], but the actual mutation rates and spectra have remained difficult to quantify precisely. We consistently observed higher chromosome copy number variation (1.52×10^{-3} events/line/generation) in HU evolved cells than in RM and YPD (Mann–Whitney U test, $p < 2.0\times10^{-6}$, Fig. 2a). The two shortest chromosomes had the most frequent copy number changes (7 chrI losses and 7 chrVI gains, Supplementary Fig. 5), both being significantly more frequent than in YPD (Fisher's exact test, $p<0.021$). Sixty-two percent of MALs in HU carried multiple chromosome gain/loss, greatly outnumbering those in YPD (7.7%, Fisher's exact test, $p=4.83\times10^{-6}$). More chromosome CNV was associated with slower growth in HU (Supplementary Fig. 6a, linear regression, $R^2=0.23$, $p=0.017$), suggesting that accumulation of aneuploidies accounts for much of the fitness loss under HU-induced mutational meltdown. Chromosome loss was associated to slower growth than chromosome gain (mean cell doubling time increase of MALs with only chromosome losses *vs.* only gains: 0.65 h vs. 0.25 h). Selection against near lethal effects of some chromosome losses likely explains why the observed rate of chromosome loss is lower than that of chromosome gain (0.45×10^{-3} vs. 1.01×10^{-3}).

In addition to the whole chromosome aneuploidies, HU evolved cells often carried large segmental duplication or loss (Fig. 3a-b), several of which associated with complex structural variation. To resolve the rearranged karyotypes, we applied long-read Nanopore sequencing to two selected MALs (SA/WE-HU-2 and SA/WE-HU-3) (STAR METHODS). We found that a large-scale non-reciprocal translocation had occurred in the SA/WE-HU-2, in which an extra copy of ~84 kb segment at chrXI left end (SA background) was translocated to chrXIV right end and had replaced the original ~150 kb copy at the right arm (SA background) (Fig. 3b-c). Such terminal CNV-associated translocation is usually generated by ectopic recombination or break-induced replication under replication stress[14,29]. The break points of these events coincided with tRNA and Ty elements, consistent with findings from previous genome instability studies of the *S. cerevisiae* deletion collection[30] and the role of Ty in mediating translocations[31]. Segmental copy number variants in SA/WE-HU-3 (Fig. 3a) were not involved in such structural rearrangements. We also identified additional insertions and deletions of substantial size (mean

length of insertion: 4913 bp, deletion: 322 bp), indicating widespread genomic instability. All of them occurred within repeat sequences, including tRNA, Ty elements, X element and Y prime in subtelomere as well as in one gene with intragenic repeats (*FLO11*). Such events were more frequent in HU than in RM (Fig. 3d), suggesting that the mutagenic effects of HU also encompass these classes of structural variants.

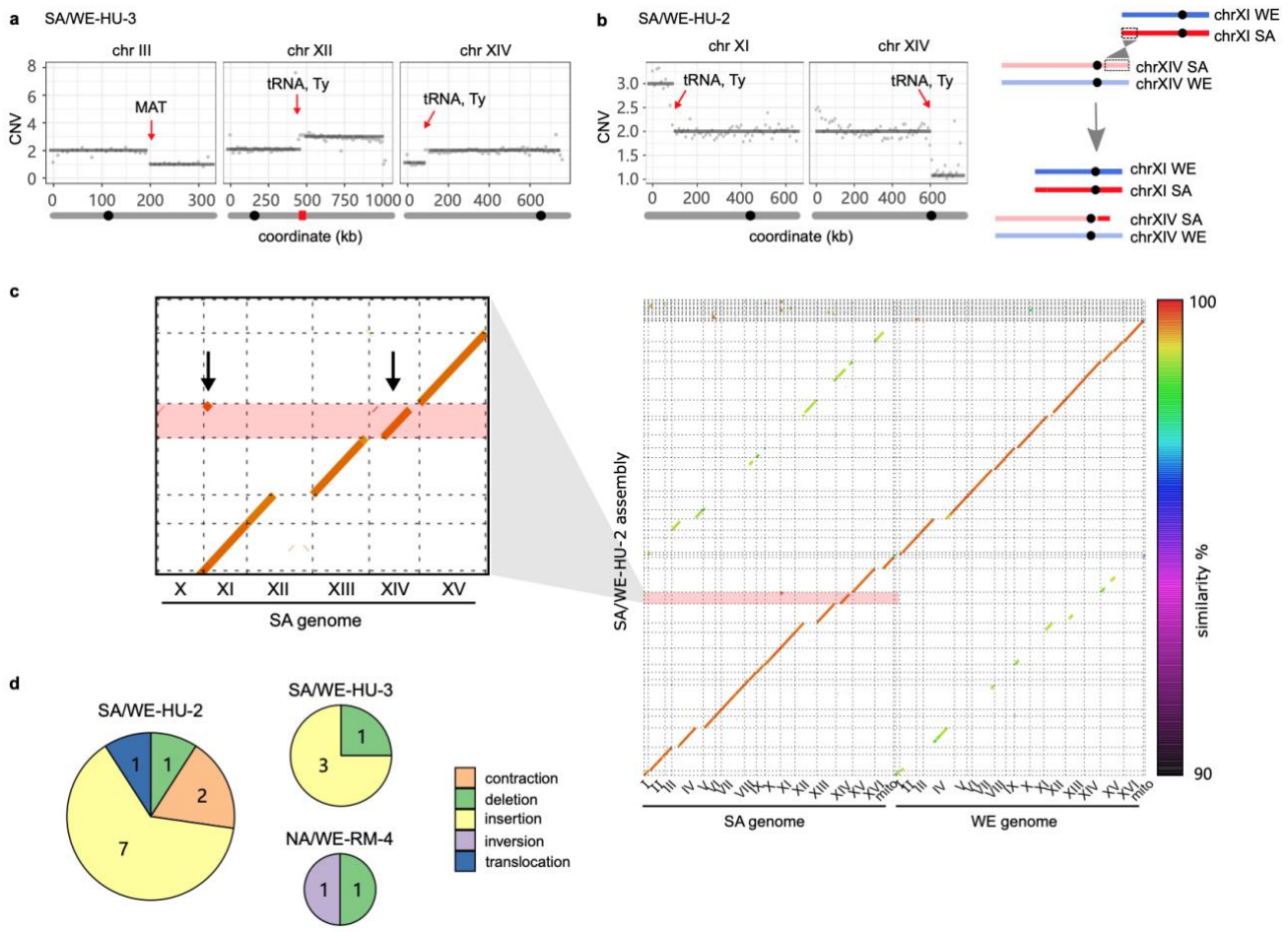

Figure 3. Segmental CNV and structural variation. (a) Segmental CNV on chrIII, chrXII and chrXIV of the SA/WE-HU-3 line by short read sequencing. **(b)** Left panel, CNV on chrXI and chrXIV of SA/WE-HU-2 line by short read sequencing. Right panel, the gained segment on chrXI right end was translocated to chrXIV left end. In panels (a) and (b), the grey bar below the coordinate represents the chromosome, on which the black circle and red rectangle indicate the location of centromere and rDNA respectively. The red arrows indicate the segmental CNV break points. **(c)** Right panel, *de novo* phased assembly of SA/WE-HU-2 line based on the long-read sequences with color to indicate the sequence similarity between the two parents. Left panel, the zoomed-in dot plots highlight one single assembled contig with SA chrXI segment translocation to chrXIV. **(d)** Global number of structural variants identified by assembly-based alignment and manual investigation in IGV (Integrative Genomics Viewer) in three long-read sequenced MALs.

Point mutation rates remain unchanged in rapamycin but are broadly elevated in HU

We next characterized single nucleotide variation (SNV) and insertion-deletion (INDEL) in YPD, RM and HU conditions. The average SNV and INDEL rates in YPD is 1.89×10^{-10} and 1.41×10^{-11} per base per generation respectively (Fig. 4a and 4c, Supplementary Fig. 7, Tables S5-S6), consistent with previous studies focused on

yeast lab strains [9–12,20]. The multiple genetic backgrounds used in our mutation accumulation allow us to investigate how mutation rate varies and whether background-specific mutational signatures exist. SNV rates in YPD varied six-fold across genetic backgrounds, supporting broad variation in spontaneous mutation rates estimated on a specific locus by fluctuation assay[22]. We focused on YPD condition where none of the ten genetic backgrounds went extinct and therefore enable us to combine results from MALs sharing a specific background (e.g., Fig. 4b, boxplot at "WE" represents SNV rates of a total of 16 MALs of WE/WE, WA/WE, NA/WE and SA/WE in YPD). We found that strains with WE genetic background had significantly higher SNV rate (Fig. 4b, Mann–Whitney U test, $p<0.05$). The proportion of observed *vs.* expected non-synonymous SNVs (74% *vs.* 76%, $p=0.59$) and genic SNVs (72% *vs.* 74%, $p=0.62$) across all genetic backgrounds supports a close-to-neutral point mutation accumulation scenario in YPD. We also measured a transition/transversion (Ts/Tv) ratio of 0.93 (expectation with no transition bias = 0.5), which is close to the previous estimates of 0.95 from a dataset of 145 MALs of common lab strains[10] and consistent with the reported general mutational bias towards transitions in yeast [9,11,20]. The C-to-T transition (30.0%), as well as the C-to-A transversion (32.4%) drove GC-to-AT bias (Fig. 4d, GC-to-AT/AT-to-GC mean = 2.58), which was also similar to that observed in previous studies[9,10].

The average SNV rate in RM (Fig. 4a, 1.80×10^{-10} per base per generation) was comparable to that in YPD (Mann–Whitney U test, $p=0.46$) while the INDEL rate (4.16×10^{-11}) was only marginally higher (Fig. 4c, Mann–Whitney U test, $p=0.01$). The proportion of non-synonymous SNVs and genic SNVs supports a neutral evolution also in RM ($p>0.33$). To confirm that RM is not mutagenic in a general sense (i.e. except in terms of chrXII amplification), we performed a canavanine-based fluctuation assay to estimate the loss-of-function mutation rate at the *CAN1* locus in the wildtype lab strain. This showed that the *CAN1* mutation rate of this wildtype strain was lower in RM (6.95×10^{-7}) and calorie restriction (CR, partially mimicking RM, 2.12×10^{-6}) compared to in the stress-free condition (3.90×10^{-6}) (Fig. 4g). The reduced *CAN1* loss-of-function mutation rate suggested that RM may enhanced activity or fidelity of components of the DNA repair machinery. To test this, we estimated the *CAN1* mutation rate across a panel of mutator strains. We found that RM could no longer rescue the mutator phenotype in the absence of *MSH2* (DNA mismatch repair), *RAD27* (base excision and non-homologous end joining repair) and *RAD51* (nucleotide excision and double stranded break repair), but not for *TSA1* (anti-oxidation activity), suggesting that the DNA repair machinery is required for RM to lower mutation rate. We found that the proportion of T-to-C and C-to-T substitutions were 1.37- and 1.41-fold higher in RM than in YPD, leading to a higher transition bias (Fig. 4e, Ts/Tv=1.52 in RM vs. 0.93 in YPD), which may reflect the activities of DNA repair pathways. Taken together, except for chrXII amplifications compensating for RM induced rDNA contractions, RM does not appear to be mutagenic and may stabilize parts of the genome with the help of common DNA repair pathways.

The average SNV and INDEL rates in HU were about six-fold higher (Tables S5-S6, Fig. 4a, SNV rate $=1.08\times10^{-9}$, $p=1.29\times10^{-11}$; Fig. 4c, INDEL rate$=9.83\times10^{-11}$, $p=4.10\times10^{-9}$) than in YPD. The fraction of non-synonymous SNVs (69.8%) was marginally lower than expected (76.0%, $p=0.03$), which may indicate a slight purifying selection. The fraction of protein coding SNVs (73.4%) was as expected (74%, $p=0.86$) under neutral

evolution. The transition bias in HU was similar to that in YPD (Ts/Tv value 1.03 vs. 0.93), but the proportion of T-to-G transversion was 3.26- fold higher (Fig. 4e), consistent with the HU mutagenic signature in *C. elegans*[32]. This mutation bias had the indirect effect of almost completely removing the general G/C-to-A/T mutational bias in yeast, which was also evident in our YPD evolved MALs (Fig. 4d, 1.13 in HU vs. 2.58 in YPD). We compared the mutation patterns observed in our HU evolved genomes to those registered in the Catalogue of Somatic Mutations in Cancer (COSMIC, https://cancer.sanger.ac.uk/cosmic/signatures) (Fig. 4e and 4f). The comparison suggested that our HU evolved cells exhibit a predominant signature of SBS9 (single base substitutions 9) and ID8 (small insertions and deletions 8), which in cancers is characteristic of DNA polymerase eta (Pol η) somatic hypermutation activity and repair of DNA double strand breaks by NHEJ (non-homologous end joining). This may reflect that HU exposed cells are forced to resort to lower fidelity DNA replication and repair processes, because of HU blocking the ribonucleotide reductase and causing a depletion of ribonucleotides[33].

More SNVs were associated with faster growth in HU (Supplementary Fig. 6b, linear regression, R^2=0.17, p=0.044), underscoring that it is the accumulation of aneuploidies and structural variation, rather than of SNVs, that accounts for the HU-induced fitness loss. This is compatible with a scenario in which a fraction of the accumulated SNVs might be favored by selection because they counteract the effects of some aneuploidies that otherwise would be lethal or near lethal. Indeed, gene ontology analysis shows that genes acquiring SNVs under HU evolution do not represent a random set of functions but are significantly enriched (p<0.0067) for genes encoding proteins binding to purine nucleotides, ribonucleotides and ribonucleoside triphosphates. Given that HU inhibits replication by inhibiting the ribonucleotide reductase[33], such enrichment makes biological sense.

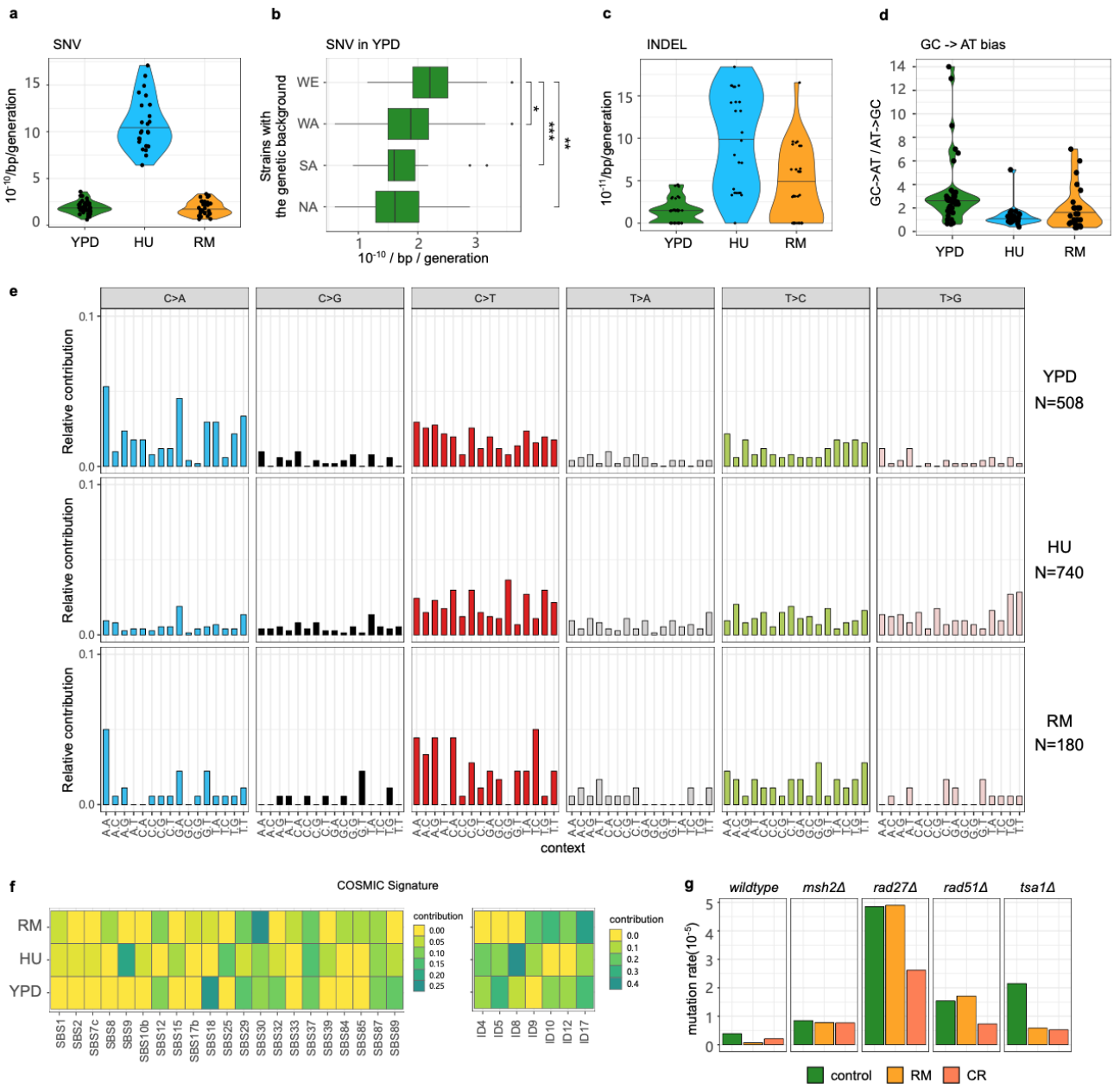

Figure 4. SNV, INDEL rates and mutational signatures. (a) SNV rate of each MALs in YPD, HU and RM. **(b)** SNV rate of YPD-evolved MALs categorized by the four parental genetic backgrounds, e.g., boxplot at "WE" represents SNV rates of a total of 16 MALs of WE/WE, WA/WE, NA/WE and SA/WE in YPD. Mann–Whitney U test is used for significance analysis. **(c)** INDEL rate of each MALs in YPD, HU and RM. **(d)** The ratio of GC-to-AT to AT-to-GC SNVs in three conditions. **(e)** Mutational profiles of MALs evolved in YPD, HU and RM based on the relative incidences of base-substitution changes within a trinucleotide context. N: the number of SNVs in each condition. **(f)** Relative contribution of COSMIC Single Base Substitution (SBS) and small insertions and deletions (ID) signatures in MALs evolved in YPD, HU and RM. **(g)** Mutation rate estimated by fluctuation assay in wildtype and four additional mutators in BY genetic background with genes responsible for DNA repair or stress response deleted. Each strain had 16 replicates. CR is short for calorie restriction.

HU is mutagenic to the mitochondrial genome

Given the huge impact of HU on virtually all nuclear mutation rates, we next estimated the copy number of mitochondrial DNA (mtDNA) to see whether the mutagenic effects encompass mtDNA deletions or loss. We

calculated the sequencing depth of three near repeat-free mitochondrial genes (*ATP6, COX2, COX3,* Fig. 5a), which avoids much of the noise arising from the AT rich and highly repetitive nature of mtDNA[34]. We found that the rate of mtDNA loss or deletion is about 10-fold higher in HU (3.47×10^{-4} mtDNA loss/line/generation) than in RM (4.73×10^{-5}) and YPD (3.29×10^{-5}). A closer look at the noisy sequencing depth along the entire mitochondria (Fig. 5b-c) reveals partial mtDNA loss (heteroplasmy), which is also more frequent in HU condition (n = 10, 1 and 2 MALs in HU, RM, and YPD). The mtDNA segments retained at normal copy numbers in these MALs ranged from 0.9 kb to 30.3 kb in size (~75-77 kb for intact mtDNA before evolution). Both mtDNA loss and deletions invariably led to *petite* colonies, reflecting a defect in oxidative phosphorylation. As yeast cells have been reported not to experience mtDNA loss under short term HU exposure (e.g. 3 days)[30], our results suggest that HU either becomes directly mtDNA mutagenic, or indirectly causes mtDNA loss (e.g. by impairing processes necessary for mtDNA maintenance), after long term exposure. Although the HU induced mtDNA losses and deletions resemble those that drive adaptation under exposure to mitochondrial superoxide[35], the HU induced mtDNA copy number changes did not associate with HU tolerance in terms of cell growth (Supplementary Fig. 6c). We also found the average mitochondrial point mutation rate to be about 10-fold higher for cells evolving in HU than in YPD and RM (4.86×10^{-4} SNVs/line/generation in HU, 3.29×10^{-5} in YPD, and 4.73×10^{-5} in RM, Fig. 5d). The elevated rates of mtDNA loss, deletions and point mutations likely reflect the lower fidelity of the mtDNA repair systems when the dNTP pool is depleted by HU[36]. Overall, we conclude that HU speeds the accumulation of a very broad range of nuclear and mitochondrial mutations and distorts the mutation spectrum, leading to cumulative errors and reduced cell fitness.

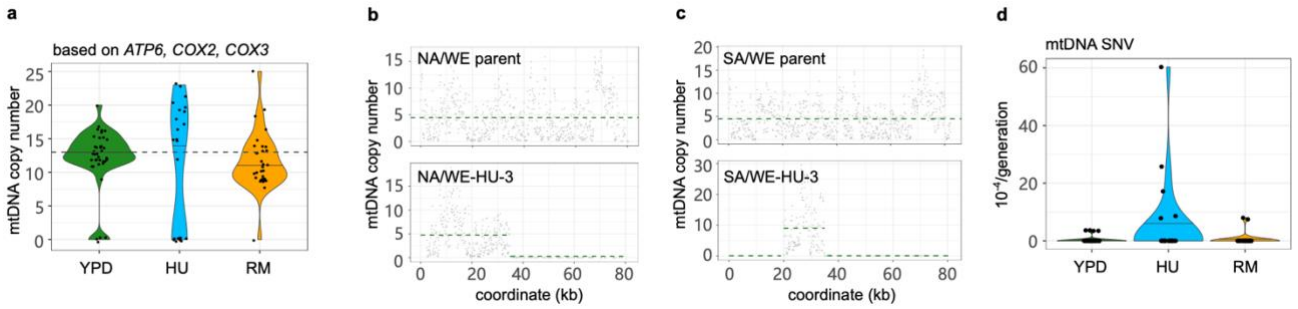

Figure 5. Mitochondrial DNA copy number. (a) Mitochondrial DNA copy number estimated by the sequencing depth of *ATP6, COX2, COX3* genes and normalized by the sequencing depth of the nuclear genome. Violin plot: center lines = median. The dashed line shows the mitochondrial copy number before evolution. **(b-c)** Mitochondrial DNA copy number of hybrid NA/WE (b) and SA/WE (c) before evolution (upper panels), and for one MAL after HU evolution (lower panels). The sequencing depth was estimated for 100 bp non-overlapping windows (dots) sliding along the mitochondrial genome (x-axis) and normalized to the sequencing depth of the nuclear genome. The dashed green line indicates the mean copy number across all windows. **(d)** SNV rate in mtDNA for the three conditions.

HU increases loss of heterozygosity (LOH) rates

Loss Of Heterozygosity (LOH) eliminates one of the parental alleles in diploid cells and allows recessive loss-of-function mutations in the remaining copy to affect phenotypes, which is broadly accepted to help driving cancer evolution and resistance development[7,37]. We mapped LOH events in MALs of the six heterozygous

strains using the MuLoYDH[12] pipeline (Fig. 6a, Supplementary Fig. 8, Table S7) and found the overall LOH rate to be significantly higher for cells evolved in HU (Fig. 6b, mean=5.75×10^{-2} per line per generation, 67 events per MAL, $p=2.29\times10^{-8}$) than in RM (mean=8.38×10^{-3} per line per generation, 11 events per MAL) and YPD (mean=5.66×10^{-3} per line per generation, 15 events per MAL). Accordingly, the rates of interstitial LOH, terminal LOH and whole chromosome loss in HU (Fig. 6c, interstitial LOH rate 4.62×10^{-2}, terminal LOH rate 1.08×10^{-2}, chromosome loss 4.94×10^{-4}) were 9.78-31.1 fold higher than in YPD and 4.88-7.02 fold higher than in RM. Overall, an average of 33.5% of the genome evolved in HU was affected by LOH at the end of evolution, compared with only 5.6% in YPD ($p=9.37\times10^{-11}$) and 6.7% in RM ($p=2.02\times10^{-10}$). In all environments, the average length of terminal LOH segments was much longer than that of the interstitial LOH segments (Fig. 6c, mean, 20.3 kb vs. 2.63 kb, $p<2.2\times10^{-16}$) and the proportion of the whole genome affected by terminal LOH was therefore 1.83~3.58 fold higher than that affected by the interstitial LOH (Fig. 6c, 20.6% vs. 11.2%, 4.52% vs. 1.41%, 4.30% vs. 1.20% in HU, RM and YPD respectively). Therefore, both the frequency of LOH and proportion of genome affected by LOH were significantly elevated in HU.

We next explored the nature of the LOH breakpoints and found their positions to agree well with those previously reported in W303/YJM789 yeast hybrid evolving in a stress-free environment[14] (Table S8). They were likely to occur in regions with high levels of gamma H2AX (phosphorylation on serine 139 of H2A histone family member X, as a reaction to DNA double-strand breaks), regions with high GC content, and in non-coding RNA genes[14]. We looked closer at the breakpoints for the recurrent LOH events on chrXII and found them to be shared independent of genetic backgrounds and conditions, coinciding with the rDNA locus and often resulting in long terminal LOHs (~600 kb) on the right arm of chrXII (Fig. 6a).

Because LOH often affects parental alleles non-randomly and drives adaptation[7,38,39], we next examined whether a parent-specific LOH bias existed and whether the occurrence of LOH was associated with improved cell growth. We compared the LOH rate and length within each hybrid, but no parental biases were detected ($p>0.06$ in all conditions). The only exception was a tendency for LOH to be longer when resulting in homo- or hemizygosity for the SA background in the SA/NA hybrid evolved in YPD ($p=0.03$), where extensive homozygosity for SA associated with faster cell growth (Supplementary Fig. 9a, linear regression, $R^2=0.9$, $p=0.052$). We also pooled the LOH events from all the hybrids involving a particular parental background to increase statistical power but found only a weak correlation between extensive homozygosity for NA and slower growth for RM evolved lineages (Supplementary Fig. 9b, $R^2=0.36$, $p=0.051$). Thus, a parent specific LOH bias was rare among our mutation accumulation lines and had limited effects.

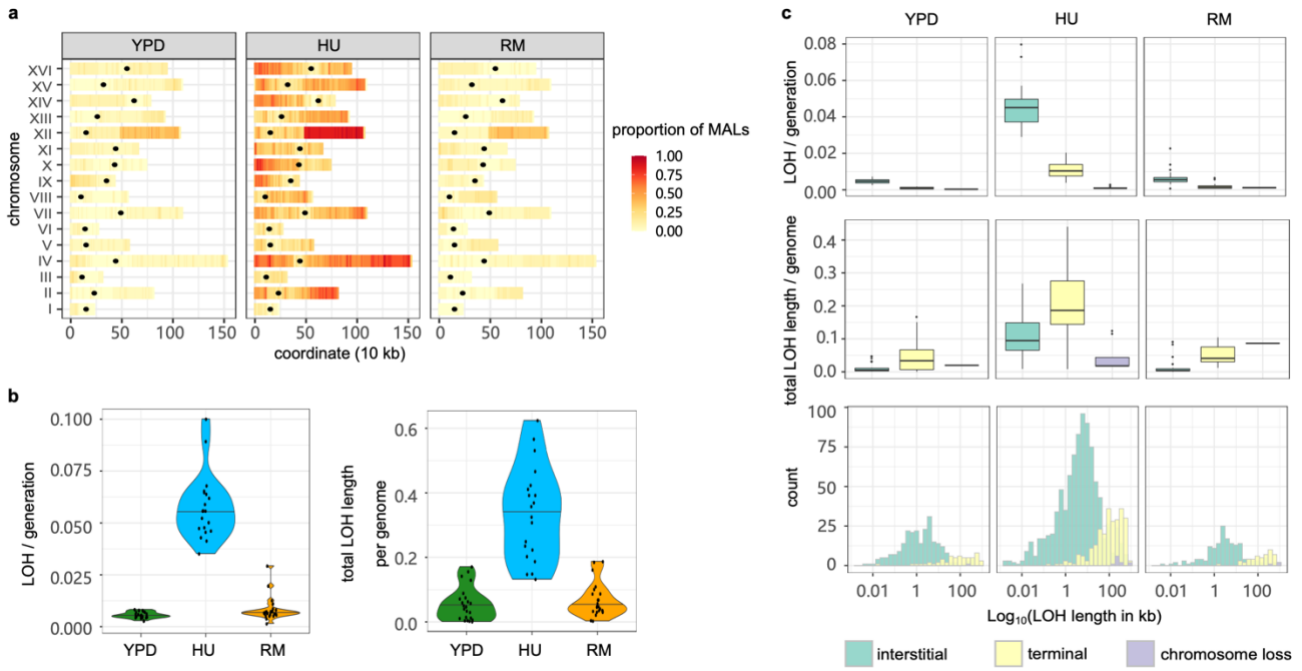

Figure 6. Loss of heterozygosity (LOH). (a) The LOH distribution landscape of all the hybrids in YPD, HU and RM conditions. The heatmap shows the proportion of MALs that have LOH events using 10 kb windows across the genome. The black circle indicates the centromere. **(b)** LOH rate (left panel) and the proportion of total LOH length in the genome (right panel) of each MAL in YPD, HU and RM. Violin plot: center lines = median. **(c)** LOH rate (upper panel), the proportion of total LOH length in the genome (middle panel) and LOH length distribution (bottom panel) for each type of LOH. Boxplot: center lines = median; boxes = interquartile range (IQR); whiskers =1.5×IQR; points = outliers beyond 1.5×IQR.

Discussion

We evolved 96 yeast lines that were propagated for a total of ~181,440 generations while passing them through regular single cell bottlenecks in drug-free, HU and RM conditions, and investigated the mutational signatures shaped by genetic backgrounds and environmental constraints. The spontaneous mutation rate and spectrum in drug-free condition mirrored previous estimates[9–11,14,20]. However, the spontaneous mutation rate varied considerably across the genetic backgrounds, showing that it is not necessarily well conserved throughout a species and should be generalized with substantial care[22]. HU is highly mutagenic and induces frequent aneuploidies leading to severe growth defects, while RM stabilizes the genome with a mutational footprint of chrXII duplication that maintains rDNA repeats homeostasis. Our findings can be relevant to the assessment of long-term genotoxic risks of cancer therapies using HU and RM.

Significant efforts have been made to infer mutational signatures across the spectrum of human cancer types, therapies and environmental mutagens[40,41], which provides insights into endogenous and exogenous causes of cancer development. However, discrimination of mutagenesis from selection is difficult when working with human samples. Highly controlled conditions and single cell bottlenecks have been used to detect mutational signatures in mammalian cell lines[3,42]. This kind of approach minimized the effects of selection but mutagen treatment (e.g., chemotherapy drugs) was often short (e.g., 24 hours) and accompanied with recover/expansion

when mutagens were removed, thereby introducing potential bias. In this study, we applied an unconventional mutation accumulation approach by imposing continuous long-term HU and RM stresses on budding yeast. We revealed unique mutational signatures like T-to-G bias in HU and chrXII duplication in RM. While comprehensive phenotyping of cell doubling time, yield and viability revealed weak or no selection, the experimental outcome was shaped by the combination of mutations rather than individual ones, as well as the experimental setup of single cell passages where individual drug survivors had to be selected. This agrees with the observation of a strong selective pressure on cell viability, where individuals carrying lethal or highly deleterious mutations are removed throughout the passages.

RM inhibits cell growth by targeting TOR, the central signaling of cell proliferation, which is conserved from yeast to human[43]. We found the genome-wide mutation rate in RM to be comparable with that in the drug-free condition, consistent with the findings in mammalian cells that inhibition of mTOR could suppress *de novo* mutations[44]. The low mutation rates were also supported by a *CAN1*-based fluctuation assay performed in this study and by another group[45]. RM might maintain genome stability by promoting DNA repair or increasing the accuracy of DNA synthesis by high fidelity polymerases. The evolution in RM also associated strongly with chrXII amplification, however, which did not confer growth advantage in RM. The chrXII amplification coincided with contraction of the rDNA repeats on this chromosome. Such RM-induced rDNA contractions are possibly near lethal, and cells can only develop into colonies to pass through single cell bottlenecks if preceded by chrXII amplifications that rescue the rDNA copy number. This is consistent with aneuploidy occurring at a rate that can emerge at small population sizes ranging from 1 to 10^6 cells for each single cell bottleneck.

In contrast to RM, HU is highly mutagenic, resulting in an increased mutation rate in all types of genomic alterations, revealing mutational signatures compatible with using low-fidelity polymerase and NHEJ for DNA replication and repair. In the absence of sex and purifying selection, such accelerated mutation rate would increase the genetic load and probably directed HU exposed populations towards mutational meltdown. As an inhibitor of ribonucleotide reductase, HU starves the cells of dNTPs and causes replication fork stalling or collapse into double strand breaks (DSBs). Frequent fork stalling can lead to un-replicated regions of DNA, which in turn cause segregation problems at anaphase[46]. This explains the observation of a high frequency of aneuploidies and segmental CNVs in HU MALs. DSBs can be repaired by cross-over or gene conversion[14,47,48], which is reflected by the frequent LOH in HU condition, as well as the ectopic translocation (Fig. 3b). The replication stress induced by HU also brings unique footprint in SNVs, with increased proportion of T-to-G transversions (19.9% in HU vs. 5.81% in YPD), which largely reverses the GC-to-AT bias commonly observed in yeast genome-wide mutations. This could be caused by unequal reduction of dNTP pools by HU or biased usage of dNTPs during replication stress. Further studies are needed to investigate the mechanisms responsible for such an AT-to-GC signature in HU.

In summary, we used the mutation accumulation experiment to characterize the mutational footprint in yeast genomes under HU, RM and drug-free conditions. Such approach allows genome-wide quantification of

genotoxic effects across different compounds and can be generalized to many environmental conditions, small molecules and drugs.

Data availability

The genomic data generated in this study are currently being submitted and will be available under the accession code PRJNA880975.

Acknowledgement

We thank Dr. Melania D'Angiolo, Marco Fumasoni and Dr. Sihai Yang for critical reading of the manuscript. We also thank Dr. Lorenzo Tattini for help with handling the long-read data and the MuLo-YDH pipeline. This work is supported by National Natural Science Foundation of China (32000395 to J. L. and 32070592 to J.-X. Y.), Natural Science Foundation of Guangdong Province (2022A1515011873 to J. L. and 2022A1515010717 to J.-X. Y.), Guangzhou Municipal Science and Technology Bureau (202102020938 to J. L.), Guangdong Basic and Applied Basic Research Foundation (2019A1515110762 to J.-X. Y.), Guangdong Pearl River Talents Program (2021QN02Y168 to J. L., 2019QN01Y183 to J.-X. Y.), Agence Nationale de la Recherche (ANR-15-IDEX-01), Fondation pour la Recherche Médicale (EQU202003010413), Association pour la Recherche sur le Cancer (ARCPJA32020070002320) to G. L.

STAR METHODS

REAGENT or RESOURCE	SOURCE	IDENTIFIER
Chemicals, Peptides, and Recombinant Proteins		
YPD Agar	MP	114001222
YPD Broth	MP	114004032
Hydroxyurea	Sigma	H8627
Rapamycin	Sigma	R8781
Canavanine	Sigma	C1625
Zymolyase	Euromedex	UZ1000
Glucose	Sigma	G8270
Yeast Nitrogen Base Without Amino Acids	Formedium	CYN0402
Complete CSM Mixture	Formedium	DCS0019
Arg drop-out	Euromedex	UD9518
Critical Commercial Assays		
MasterPure Yeast DNA Purification Kit	Epicentre	MPY80200
Oxford Nanopore Sequencing kit	ONT	SQK-LSK109
Oxford Nanopore Barcoding kit	ONT	EXP-NBD104
Yeast HMW DNA Extraction	Qiagen	Genomic-tip 100/G
RNeasy Mini Kit	Qiagen	74104
PrimeScript RT reagent kit with gDNA Eraser	TaKaRa	RR047A
TB Green Premix Ex Taq™ II	TaKaRa	RR820A
Premix Taq DNA Polymerase	TaKaRa	R004A
Deposited Data		
Raw sequencing reads		PRJNA880975
Experimental Models: Organisms/Strains		
DBVPG6765	1002 yeast genome project	Table S1
DBVPG6044	1002 yeast genome project	Table S1
YPS128	1002 yeast genome project	Table S1
Y12	1002 yeast genome project	Table S1

Software and Algorithms		
MuLoYDH	Tattini et al, 2019	https://bitbucket.org/lt11/muloydhom
Varathon		https://github.com/yjx1217/Varathon
MutationalPatterns	Manders et al, 2022	https://bioconductor.org/packages/release/bioc/html/MutationalPatterns.html
Scan-o-Matic	Zackrisson et al, 2016	https://github.com/Scan-o-Matic/scanomatic
bz-rate	Gillet-Markowska et al, 2015	http://www.lcqb.upmc.fr/bzrates
regioneR	Gel et al, 2016	https://www.bioconductor.org/packages/release/bioc/html/regioneR.html
Liftoff	Shumate et al, 2021	https://github.com/agshumate/Liftoff

METHOD DETAILS

Mutation accumulation experiments and genome sequencing

The details of strains and all the mutation accumulation lines are listed in Table S1. Briefly, ten diploid strains used in this study are derived from DBVPG6044 (West African, WA), DBVPG6765 (Wine/European, WE), YPS128 (North American, NA), and Y12 (Sake, SA), either in homozygous or heterozygous state. We propagated mutation accumulation lines (MALs) in YPD (2% peptone, 1% yeast extract, 2% glucose, 2% agar), hydroxyurea (HU, 10 mg/ml) and rapamycin (RM, 0.025 ug/ml) conditions by streaking to single colonies at fixed time intervals (2 days for YPD and 4 days for HU and RM, respectively) and letting them grow at 30 °C in a static incubator. We propagated four independent replicates for each genetic background. All the genetic backgrounds were used for MALs in YPD while two of them (WA/WA, WE/WE) were excluded in HU and RM due to low viability and severe growth defects. The Sake (SA/SA) homozygotes and SA/WA hybrids died out during mutation accumulation in HU. Therefore, there are a total of 40, 24 and 32 MALs in YPD, HU and RM, that were propagated for 120, 60 and 60 single-cell bottlenecks, respectively. We stored all the samples at five intermediate timepoints across the experiments as fossil records (single-cell bottleneck 0, 30, 60, 90, 120 in YPD; single-cell bottleneck 0, 15, 30, 45, 60 in HU and RM).

We estimated the number of generations between bottlenecks by counting the cell number (N) of the colonies using the hemocytometer. We assume that a single colony is derived from a single cell by continuous dividing without cell death. The generations between bottlenecks (G) equal $\log_2(N)$. We estimated G for all the ancestors at P0 (G_{P0}) in YPD, HU and RM conditions and for MALs at the last time point in the conditions in which they evolved (G_{P60} in HU or RM; G_{P120} in YPD). We used the mean value of G at P0 and the last time point to represent the number of generations between bottlenecks across the mutation accumulation experiments. Overall, we estimated 23 generations every 2 days for YPD, 20 generations every 4 days for HU, 22 generations every 4 days for RM, that accounted for a total of 2760, 1200 and 1320 generations across the MAL experiment for YPD, HU and RM, respectively.

The genomic DNA of all the ancestors and clones at the last timepoint was extracted with the "Yeast MasterPure" kit (Epicentre, USA) according to the manufacturer's instructions. All these samples were sequenced by Illumina technology at Ginkgo Bioworks (Boston, Massachusetts, United States).

Genomic data analysis

We applied an established pipeline "MuLoYDH"[12] that is designed for accurately tracking the mutational landscape of yeast diploids. The scripts for read mapping, coverage calculation, CNV calling and annotation, SNV and INDEL calling and annotation, LOH detection and annotation are all embedded in MuLoYDH, which can be downloaded via https://bitbucket.org/lt11/muloydhom. For SNV annotation we used the following criteria: i) All the SNVs must be called by both Freebayes and Samtools; ii) The quality score of each SNV must be higher than 50 and sequencing depth at that locus must be higher than 10X; iii) Each SNV must be supported by at least 6 reads including both forward and reverse reads. Repeat sequences such as telomeric regions were excluded. Moreover, SNVs existing in the ancestral genomes were filtered out. All SNVs and INDELs that passed these filters were visually checked in the Integrative Genomics Viewer (IGV). The ancestral genomes of WA, WE, SA and NA[49] (https://yjx1217.github.io/Yeast_PacBio_2016/data/) were processed by the R package BSgenome (version 1.66.1, https://bioconductor.org/packages/BSgenome) to forge the corresponding reference genome packages. Then, the SNV and INDEL mutational signatures were analyzed and fit to the COSMIC signatures using the R/Bioconductor MutationalPatterns package[50], in which a strict refitting function "fit_to_signatures_strict" and a cutoff of 0.004 were applied.

In order to systematically estimate the CNV of rDNA, we applied the modules 01. Short_Read_Mapping and 04.Short_Read_CNV_Calling of the pipeline "Varathon" (https://github.com/yjx1217/Varathon). Of note, here we used a modified SGD reference which contains only one copy of the rDNA region on chrXII. The estimated copy number of rDNA for each MAL was normalized by that of its ancestor.

LOH association analysis

LOH was profiled by MuLoYDH[12]. We used "start-(first-start) ~ first" and "last ~ end+(end-last)" to define upstream and downstream breakpoints of each LOH event. We used "start ~ end" to define the LOH tracts. When analyzing the association between LOH breakpoints and published datasets and genomic features, we excluded the MALs of haploid and tetraploid. We also excluded LOH presented by only one single marker. We lift over the LOH break points as well as the Spo11 hotspots[51] and meiotic recombination hotspots[52] from their original reference to the SGD reference (S288C_reference_genome_R64-1-1_20110203) by Liftoff[53]. We performed permutation tests to see if the overlap between our LOH break points dataset and published datasets is higher than expected by chance using overlapPermTest function (ntimes = 1000, and alternative = "greater") in regioneR package[54]. The output of *p* value was listed in Table S8.

Long-read sequencing and data analysis

We applied Oxford Nanopore Technologies (ONT) on three MALs which showed potential structural variation (SV) based on the Illumina sequencing. High-molecular weight (HMW) DNA was prepared by QIAGEN Genomic-tip 100/G. We started with 2 ug HMW DNA to prepare the sequencing library. DNA repair and end preparation were performed using the following reaction setup: 48 ul DNA, 3.5 ul NEBNext FFPE DNA Repair Buffer, 2 ul NEBNext FFPE DNA Repair Mix, 3.5 ul UltraII End-prep reaction buffer and 3 ul UltraII End-prep enzyme mix, which was incubated at 20 °C for 15 minutes followed by 65 °C for 15 minutes. After AMPure XP Beads clean-up (1:1 ratio), different native barcodes (ONT, EXP-NBD104) were ligated to each sample (22.5 ul DNA, 2.5 ul Native Barcode and 25 ul Blunt/TA ligase Master Mix, incubated at 25 °C for 20 minutes). After AMPure XP Beads clean-up (1:1 ratio), multiple barcoded samples were pooled and sequencing adaptor was ligated to the pooled library (65 ul pooled DNA, 5 ul AMII, 20 ul NEBNext Quick ligation reaction buffer, 10 ul Quick T4 DNA ligase, incubated at 25 °C for 15 minutes). Following AMPure XP Beads clean-up (0.4X) and L Fragment Buffer wash (ONT, SQK-LSK109), the library was eluted in 15 ul Elution Buffer. The library was loaded into the FLO-MIN106 MinION flow cell according to the manufacturer's guidelines (ONT, SQK-LSK109) to perform the whole-genome long-read sequencing.

The raw nanopore reads were processed using the 00.Long_Reads module of the LRSDAY v1.5.0 framework[55]. Briefly, we performed base calling and demultiplexing with Guppy v2.3.5. The demultiplexed reads were further processed by Porechop v0.2.4 (https://github.com/rrwick/Porechop) for adaptor trimming (option: –discard_middle). The *de novo* assembly was carried out by the 01.Long-read-based_Genome_Assembly module of LRSDAY. We used "canu" as the assembler (Koren et al, 2017; https://github.com/marbl/canu). SVs were called by MUM&Co[56], which uses Whole Genome Alignment information provided by MUMmer (v4) to detect variants. The SVs were further crossvalidated with the results called by the module 11.Long_Read_Mapping of the pipeline "Varathon" (https://github.com/yjx1217/Varathon) and manually checked in IGV.

Phenotyping

We revived the intermediate samples of MALs and phenotyped them by measuring their doubling time and yield. We used a high-resolution large-scale scanning platform, Scan-o-matic, to monitor cell growth in a 1536-colony design on solid agar plate[57]. The Scan-o-matic program uses data from the time-series images taken by the high-quality desktop scanners to calculate the population size and generate growth curves for the colonies. Phenotyping was run for 3 days, and scans were continuously performed every 20 minutes. The conditions of phenotyping were the same as that in the mutation accumulation experiments. Each sample had at least 6 technical replicates. After quality control filtering, the measurement of doubling time was extracted for downstream analysis in R (R version 3.6.3). Yield used in the paper was a log2 ratio between a surface of the assay position and the spatial controls. All the scripts are available on GitHub (https://github.com/Scan-o-Matic/scanomatic; last accessed September 1, 2020).

Viability estimation

To estimate the cell viability in drug conditions, we cultured cells in liquid YPD until they reached mid-log phase and then diluted the culture to plate ~200 cells on solid medium with or without drugs. After incubation at 30 °C for 4 days, we counted colony-forming units (CFU) and calculated the viability based on the ratio of CFU in HU/RM and YPD control conditions. To estimate the viability in YPD condition, we measured CFU on YPD plates using the same approach as described above. Each strain had four replicates. Meanwhile, we count the cells under the microscope by hemocytometer. After transforming CFU and counted cell number to the same dilution scale, viability was calculated by CFU divided by cell number.

Fluctuation assay

The protocols of Luria-Delbrück fluctuation assay[58] were applied to determine the mutation rate at which the cells become resistant to canavanine (60 ug/ml) in different conditions. The strains used for this experiment were gifts from Dr. Alain G. Nicolas[15]. Briefly, 16 clones of each strain were picked, then independently diluted to ~100 cells and cultured in SC (2% glucose, 0.675% yeast nitrogen base, 0.088% complete amino acid supplement, pH=6.0), SC+RM (0,025 μg/mL) and SC with calorie restriction (0.5% instead of 2% glucose), respectively. After four days of incubation at 30 °C, we spotted the cultured cells on the over-dried canavanine plates, as well as the SC plates as control, using an appropriate dilution to avoid too many or too few cells. After three days of incubation, we counted the resistant colonies and inferred the number of mutants and total cells in the culture of SC, RM and calorie restriction. We used an online tool "bz-rate" to calculate the mutation rate for different conditions[59] (http://www.lcqb.upmc.fr/bzrates).

References

1. Lee, J.-K., Choi, Y.-L., Kwon, M., and Park, P.J. (2016). Mechanisms and Consequences of Cancer Genome Instability: Lessons from Genome Sequencing Studies. Annual Review of Pathology: Mechanisms of Disease *11*, 283–312. 10.1146/annurev-pathol-012615-044446.
2. Pich, O., Muiños, F., Lolkema, M.P., Steeghs, N., Gonzalez-Perez, A., and Lopez-Bigas, N. (2019). The mutational footprints of cancer therapies. Nat Genet *51*, 1732–1740. 10.1038/s41588-019-0525-5.
3. Kucab, J.E., Zou, X., Morganella, S., Joel, M., Nanda, A.S., Nagy, E., Gomez, C., Degasperi, A., Harris, R., Jackson, S.P., et al. (2019). A Compendium of Mutational Signatures of Environmental Agents. Cell *177*, 821-836.e16. 10.1016/j.cell.2019.03.001.
4. Lang, G.I., Rice, D.P., Hickman, M.J., Sodergren, E., Weinstock, G.M., Botstein, D., and Desai, M.M. (2013). Pervasive genetic hitchhiking and clonal interference in forty evolving yeast populations. Nature *500*, 571–574. 10.1038/nature12344.
5. Burke, M.K., Liti, G., and Long, A.D. (2014). Standing Genetic Variation Drives Repeatable Experimental Evolution in Outcrossing Populations of Saccharomyces cerevisiae. Mol Biol Evol *31*, 3228–3239. 10.1093/molbev/msu256.
6. Levy, S.F., Blundell, J.R., Venkataram, S., Petrov, D.A., Fisher, D.S., and Sherlock, G. (2015). Quantitative evolutionary dynamics using high-resolution lineage tracking. Nature *519*, 181–186. 10.1038/nature14279.
7. Vázquez-García, I., Salinas, F., Li, J., Fischer, A., Barré, B., Hallin, J., Bergström, A., Alonso-Perez, E., Warringer, J., Mustonen, V., et al. (2017). Clonal Heterogeneity Influences the Fate of New Adaptive Mutations. Cell Reports *21*, 732–744. 10.1016/j.celrep.2017.09.046.
8. Li, J., Vázquez-García, I., Persson, K., González, A., Yue, J.-X., Barré, B., Hall, M.N., Long, A., Warringer, J., Mustonen, V., et al. (2019). Shared Molecular Targets Confer Resistance over Short and Long Evolutionary Timescales. Molecular Biology and Evolution *36*, 691–708. 10.1093/molbev/msz006.

9. Lynch, M., Sung, W., Morris, K., Coffey, N., Landry, C.R., Dopman, E.B., Dickinson, W.J., Okamoto, K., Kulkarni, S., Hartl, D.L., et al. (2008). A genome-wide view of the spectrum of spontaneous mutations in yeast. PNAS *105*, 9272–9277. 10.1073/pnas.0803466105.

10. Zhu, Y.O., Siegal, M.L., Hall, D.W., and Petrov, D.A. (2014). Precise estimates of mutation rate and spectrum in yeast. PNAS *111*, E2310–E2318. 10.1073/pnas.1323011111.

11. Sharp, N.P., Sandell, L., James, C.G., and Otto, S.P. (2018). The genome-wide rate and spectrum of spontaneous mutations differ between haploid and diploid yeast. PNAS *115*, E5046–E5055. 10.1073/pnas.1801040115.

12. Tattini, L., Tellini, N., Mozzachiodi, S., D'Angiolo, M., Loeillet, S., Nicolas, A., and Liti, G. (2019). Accurate Tracking of the Mutational Landscape of Diploid Hybrid Genomes. Molecular Biology and Evolution *36*, 2861–2877. 10.1093/molbev/msz177.

13. Loeillet, S., Herzog, M., Puddu, F., Legoix, P., Baulande, S., Jackson, S.P., and Nicolas, A.G. (2020). Trajectory and uniqueness of mutational signatures in yeast mutators. PNAS *117*, 24947–24956. 10.1073/pnas.2011332117.

14. Sui, Y., Qi, L., Wu, J.-K., Wen, X.-P., Tang, X.-X., Ma, Z.-J., Wu, X.-C., Zhang, K., Kokoska, R.J., Zheng, D.-Q., et al. (2020). Genome-wide mapping of spontaneous genetic alterations in diploid yeast cells. PNAS. 10.1073/pnas.2018633117.

15. Serero, A., Jubin, C., Loeillet, S., Legoix-Né, P., and Nicolas, A.G. (2014). Mutational landscape of yeast mutator strains. PNAS *111*, 1897–1902. 10.1073/pnas.1314423111.

16. Li, J., Rinnerthaler, M., Hartl, J., Weber, M., Karl, T., Breitenbach-Koller, H., Mülleder, M., Vowinckel, J., Marx, H., Sauer, M., et al. (2020). Slow Growth and Increased Spontaneous Mutation Frequency in Respiratory Deficient afo1-Yeast Suppressed by a Dominant Mutation in ATP3. G3: Genes, Genomes, Genetics *10*, 4637–4648. 10.1534/g3.120.401537.

17. Chen, G., Bradford, W.D., Seidel, C.W., and Li, R. (2012). Hsp90 stress potentiates rapid cellular adaptation through induction of aneuploidy. Nature *482*, 246–250. 10.1038/nature10795.

18. Shor, E., Fox, C.A., and Broach, J.R. (2013). The Yeast Environmental Stress Response Regulates Mutagenesis Induced by Proteotoxic Stress. PLOS Genetics *9*, e1003680. 10.1371/journal.pgen.1003680.

19. van Dijk, D., Dhar, R., Missarova, A.M., Espinar, L., Blevins, W.R., Lehner, B., and Carey, L.B. (2015). Slow-growing cells within isogenic populations have increased RNA polymerase error rates and DNA damage. Nat Commun *6*, 7972. 10.1038/ncomms8972.

20. Liu, H., and Zhang, J. (2019). Yeast Spontaneous Mutation Rate and Spectrum Vary with Environment. Current Biology *29*, 1584-1591.e3. 10.1016/j.cub.2019.03.054.

21. Voordeckers, K., Colding, C., Grasso, L., Pardo, B., Hoes, L., Kominek, J., Gielens, K., Dekoster, K., Gordon, J., Van der Zande, E., et al. (2020). Ethanol exposure increases mutation rate through error-prone polymerases. Nat Commun *11*, 3664. 10.1038/s41467-020-17447-3.

22. Jiang, P., Ollodart, A.R., Sudhesh, V., Herr, A.J., Dunham, M.J., and Harris, K. (2021). A modified fluctuation assay reveals a natural mutator phenotype that drives mutation spectrum variation within Saccharomyces cerevisiae. eLife *10*, e68285. 10.7554/eLife.68285.

23. Cubillos, F.A., Parts, L., Salinas, F., Bergström, A., Scovacricchi, E., Zia, A., Illingworth, C.J.R., Mustonen, V., Ibstedt, S., Warringer, J., et al. (2013). High-Resolution Mapping of Complex Traits with a Four-Parent Advanced Intercross Yeast Population. Genetics *195*, 1141–1155. 10.1534/genetics.113.155515.

24. Heasley, L.R., Watson, R.A., and Argueso, J.L. (2020). Punctuated Aneuploidization of the Budding Yeast Genome. Genetics *216*, 43–50. 10.1534/genetics.120.303536.

25. Peter, J., Chiara, M.D., Friedrich, A., Yue, J.-X., Pflieger, D., Bergström, A., Sigwalt, A., Barre, B., Freel, K., Llored, A., et al. (2018). Genome evolution across 1,011 Saccharomyces cerevisiae isolates. Nature *556*, 339–344. 10.1038/s41586-018-0030-5.

26. Jack, C.V., Cruz, C., Hull, R.M., Keller, M.A., Ralser, M., and Houseley, J. (2015). Regulation of ribosomal DNA amplification by the TOR pathway. PNAS *112*, 9674–9679. 10.1073/pnas.1505015112.

27. Lyu, X., Chastain, M., and Chai, W. (2019). Genome-wide mapping and profiling of γH2AX binding hotspots in response to different replication stress inducers. BMC Genomics *20*, 579. 10.1186/s12864-019-5934-4.

28. Barlow, J.H., Faryabi, R.B., Callén, E., Wong, N., Malhowski, A., Chen, H.T., Gutierrez-Cruz, G., Sun, H.-W., McKinnon, P., Wright, G., et al. (2013). Identification of Early Replicating Fragile Sites that Contribute to Genome Instability. Cell *152*, 620–632. 10.1016/j.cell.2013.01.006.

29. Zheng, D.-Q., Zhang, K., Wu, X.-C., Mieczkowski, P.A., and Petes, T.D. (2016). Global analysis of genomic instability caused by DNA replication stress in Saccharomyces cerevisiae. Proceedings of the National Academy of Sciences *113*, E8114–E8121. 10.1073/pnas.1618129113.

30. Puddu, F., Herzog, M., Selivanova, A., Wang, S., Zhu, J., Klein-Lavi, S., Gordon, M., Meirman, R., Millan-Zambrano, G., Ayestaran, I., et al. (2019). Genome architecture and stability in the Saccharomyces cerevisiae knockout collection. Nature *573*, 416–420. 10.1038/s41586-019-1549-9.

31. Breilmann, D., Gafner, J., and Ciriacy, M. (1985). Gene conversion and reciprocal exchange in a Ty-mediated translocation in yeast. Curr Genet *9*, 553–560. 10.1007/BF00381167.

32. Volkova, N.V., Meier, B., González-Huici, V., Bertolini, S., Gonzalez, S., Vöhringer, H., Abascal, F., Martincorena, I., Campbell, P.J., Gartner, A., et al. (2020). Mutational signatures are jointly shaped by DNA damage and repair. Nature Communications *11*, 2169. 10.1038/s41467-020-15912-7.

33. Koç, A., Wheeler, L.J., Mathews, C.K., and Merrill, G.F. (2004). Hydroxyurea Arrests DNA Replication by a Mechanism That Preserves Basal dNTP Pools *. Journal of Biological Chemistry *279*, 223–230. 10.1074/jbc.M303952200.

34. De Chiara, M., Friedrich, A., Barré, B., Breitenbach, M., Schacherer, J., and Liti, G. (2020). Discordant evolution of mitochondrial and nuclear yeast genomes at population level. BMC Biol *18*, 1–15. 10.1186/s12915-020-00786-4.

35. Stenberg, S., Li, J., Gjuvsland, A.B., Persson, K., Demitz-Helin, E., Peña, C.G., Yue, J.-X., Gilchrist, C., Ärengård, T., Ghiaci, P., et al. (2021). Genetically controlled mtDNA editing prevents ROS damage by arresting oxidative phosphorylation. 2020.11.20.391110. 10.1101/2020.11.20.391110.

36. Wanrooij, P.H., Engqvist, M.K.M., Forslund, J.M.E., Navarrete, C., Nilsson, A.K., Sedman, J., Wanrooij, S., Clausen, A.R., and Chabes, A. (2017). Ribonucleotides incorporated by the yeast mitochondrial DNA polymerase are not repaired. Proc Natl Acad Sci U S A *114*, 12466–12471. 10.1073/pnas.1713085114.

37. McGranahan, N., Rosenthal, R., Hiley, C.T., Rowan, A.J., Watkins, T.B.K., Wilson, G.A., Birkbak, N.J., Veeriah, S., Loo, P.V., Herrero, J., et al. (2017). Allele-Specific HLA Loss and Immune Escape in Lung Cancer Evolution. Cell *171*, 1259-1271.e11. 10.1016/j.cell.2017.10.001.

38. Lancaster, S.M., Payen, C., Heil, C.S., and Dunham, M.J. (2019). Fitness benefits of loss of heterozygosity in Saccharomyces hybrids. Genome Res. *29*, 1685–1692. 10.1101/gr.245605.118.

39. Smukowski Heil, C.S., DeSevo, C.G., Pai, D.A., Tucker, C.M., Hoang, M.L., and Dunham, M.J. (2017). Loss of Heterozygosity Drives Adaptation in Hybrid Yeast. Molecular Biology and Evolution *34*, 1596–1612. 10.1093/molbev/msx098.

40. Alexandrov, L.B., Kim, J., Haradhvala, N.J., Huang, M.N., Tian Ng, A.W., Wu, Y., Boot, A., Covington, K.R., Gordenin, D.A., Bergstrom, E.N., et al. (2020). The repertoire of mutational signatures in human cancer. Nature *578*, 94–101. 10.1038/s41586-020-1943-3.

41. Koh, G., Degasperi, A., Zou, X., Momen, S., and Nik-Zainal, S. (2021). Mutational signatures: emerging concepts, caveats and clinical applications. Nat Rev Cancer *21*, 619–637. 10.1038/s41568-021-00377-7.

42. Szikriszt, B., Póti, Á., Pipek, O., Krzystanek, M., Kanu, N., Molnár, J., Ribli, D., Szeltner, Z., Tusnády, G.E., Csabai, I., et al. (2016). A comprehensive survey of the mutagenic impact of common cancer cytotoxics. Genome Biology *17*, 99. 10.1186/s13059-016-0963-7.

43. Loewith, R., and Hall, M.N. (2011). Target of Rapamycin (TOR) in Nutrient Signaling and Growth Control. Genetics *189*, 1177–1201. 10.1534/genetics.111.133363.

44. Shen, C., Oswald, D., Phelps, D., Cam, H., Pelloski, C.E., Pang, Q., and Houghton, P.J. (2013). Regulation of FANCD2 by the mTOR Pathway Contributes to the Resistance of Cancer Cells to DNA Double-Strand Breaks. Cancer Res *73*, 3393–3401. 10.1158/0008-5472.CAN-12-4282.

45. Su, W.-H., Chan, C.E.T., Lian, T., Biju, M., Miura, A., Alkhafaji, S.A., Do, K.K., Latifi, B., Nguyen, T.T., and Schriner, S.E. (2021). Protection of nuclear DNA by lifespan-extending compounds in the yeast Saccharomyces cerevisiae. Mutation Research/Fundamental and Molecular Mechanisms of Mutagenesis *822*, 111738. 10.1016/j.mrfmmm.2021.111738.

46. Wilhelm, T., Magdalou, I., Barascu, A., Técher, H., Debatisse, M., and Lopez, B.S. (2014). Spontaneous slow replication fork progression elicits mitosis alterations in homologous recombination-deficient mammalian cells. PNAS *111*, 763–768. 10.1073/pnas.1311520111.

47. Saintigny, Y., Delacôte, F., Varès, G., Petitot, F., Lambert, S., Averbeck, D., and Lopez, B.S. (2001). Characterization of homologous recombination induced by replication inhibition in mammalian cells. EMBO J *20*, 3861–3870. 10.1093/emboj/20.14.3861.

48. Petermann, E., Orta, M.L., Issaeva, N., Schultz, N., and Helleday, T. (2010). Hydroxyurea-stalled replication forks become progressively inactivated and require two different RAD51-mediated pathways for restart and repair. Mol. Cell *37*, 492–502. 10.1016/j.molcel.2010.01.021.

49. Yue, J.-X., Li, J., Aigrain, L., Hallin, J., Persson, K., Oliver, K., Bergström, A., Coupland, P., Warringer, J., Lagomarsino, M.C., et al. (2017). Contrasting evolutionary genome dynamics between domesticated and wild yeasts. Nature Genetics *49*, 913–924. 10.1038/ng.3847.

50. Manders, F., Brandsma, A.M., de Kanter, J., Verheul, M., Oka, R., van Roosmalen, M.J., van der Roest, B., van Hoeck, A., Cuppen, E., and van Boxtel, R. (2022). MutationalPatterns: the one stop shop for the analysis of mutational processes. BMC Genomics *23*, 134. 10.1186/s12864-022-08357-3.

51. Pan, J., Sasaki, M., Kniewel, R., Murakami, H., Blitzblau, H.G., Tischfield, S.E., Zhu, X., Neale, M.J., Jasin, M., Socci, N.D., et al. (2011). A hierarchical combination of factors shapes the genome-wide topography of yeast meiotic recombination initiation. Cell *144*, 719–731. 10.1016/j.cell.2011.02.009.

52. Mancera, E., Bourgon, R., Brozzi, A., Huber, W., and Steinmetz, L.M. (2008). High-resolution mapping of meiotic crossovers and non-crossovers in yeast. Nature *454*, 479–485. 10.1038/nature07135.

53. Shumate, A., and Salzberg, S.L. (2021). Liftoff: accurate mapping of gene annotations. Bioinformatics *37*, 1639–1643. 10.1093/bioinformatics/btaa1016.

54. Gel, B., Díez-Villanueva, A., Serra, E., Buschbeck, M., Peinado, M.A., and Malinverni, R. (2016). regioneR: an R/Bioconductor package for the association analysis of genomic regions based on permutation tests. Bioinformatics *32*, 289–291. 10.1093/bioinformatics/btv562.

55. Yue, J.-X., and Liti, G. (2018). Long-read sequencing data analysis for yeasts. Nat Protoc *13*, 1213–1231. 10.1038/nprot.2018.025.

56. O'Donnell, S., and Fischer, G. (2020). MUM&Co: accurate detection of all SV types through whole-genome alignment. Bioinformatics *36*, 3242–3243. 10.1093/bioinformatics/btaa115.

57. Zackrisson, M., Hallin, J., Ottosson, L.-G., Dahl, P., Fernandez-Parada, E., Ländström, E., Fernandez-Ricaud, L., Kaferle, P., Skyman, A., Stenberg, S., et al. (2016). Scan-o-matic: High-Resolution Microbial Phenomics at a Massive Scale. G3, g3.116.032342. 10.1534/g3.116.032342.

58. Lang, G.I., and Murray, A.W. (2008). Estimating the Per-Base-Pair Mutation Rate in the Yeast Saccharomyces cerevisiae. Genetics *178*, 67–82. 10.1534/genetics.107.071506.

59. Gillet-Markowska, A., Louvel, G., and Fischer, G. (2015). bz-rates: A Web Tool to Estimate Mutation Rates from Fluctuation Analysis. G3 Genes|Genomes|Genetics *5*, 2323–2327. 10.1534/g3.115.019836.